

Crane: An Accurate and Scalable Neural Sketch for Graph Stream Summarization

Boyan Wang
Hefei University of
Technology, Hefei, China
wangboyan@mail.hfut.edu.cn

Zhuochen Fan
Pengcheng Laboratory
Shenzhen, China
fanzc@pku.edu.cn

Zeyu Luan
Pengcheng Laboratory
Shenzhen, China
luanz@pcl.ac.cn

Lei Zou
Peking University
Beijing, China
zoulei@pku.edu.cn

Dayu Wang
Nanyang Technological
University, Singapore
dayu001@e.ntu.edu.sg

Fangcheng Fu
Shanghai Jiao Tong
University
Shanghai, China
ccchengff@sjtu.edu.cn

Qing Li
Pengcheng Laboratory
Shenzhen, China
liq@pcl.ac.cn

Tong Yang
Peking University
Beijing, China
yangtong@pku.edu.cn

ABSTRACT

Graph streams are rapidly evolving sequences of edges that convey continuously changing relationships among entities, playing a crucial role in domains such as networking, finance, and cybersecurity. Their massive scale and high dynamism make obtaining accurate statistics challenging with limited memory constraints. Traditional methods summarize graph streams through hand-crafted sketches, while recent studies have begun to replace these sketches with neural counterparts to improve adaptability and accuracy. However, this shift faces a major challenge: under limited memory, dominant frequent items tend to overshadow rare ones, hindering the neural network's ability to recover accurate statistics. To address this, we propose *Crane*, a hierarchical neural sketch architecture for graph stream summarization. Crane uses a hierarchical carry mechanism that automatically elevates frequent items to higher memory layers, reducing interference between frequent and infrequent items within the same layer. To better accommodate real-world deployment, Crane further adopts an adaptive memory expansion strategy that dynamically adds new layers once the occupancy of the top layer exceeds a threshold, enabling scalability across diverse data magnitudes. Extensive experiments on various datasets ranging from 20K to 60M edges demonstrate that Crane reduces estimation error by roughly 10 \times compared to state-of-the-art methods.

1 INTRODUCTION

1.1 Background and Motivation

Graph streams, as time-ordered sequences of edge updates, encapsulate the continuously evolving relationships among entities in dynamic systems. Formally, a graph stream S_G is defined as a sequence $\{e_1, e_2, \dots, e_i, \dots\}$, where each item e_i represents a directed edge from an origin node o_i to a destination node d_i , augmented with a varying weight w_i at timestamp i . This model accommodates repeated edges with varying weights over time, enabling the accumulation of edge strengths and the construction of a dynamically extending graph $G(V, E)$ that reflects ongoing interconnections or interactions among entities. Such representations are particularly suited for high-velocity data environments and have found widespread applications in big data domains [1–4], including network security [5–8], financial transaction analysis [9–12], social network analysis [13–16], and beyond, where scalability and adaptability to streaming inputs are paramount.

Recently, there has been a notable shift in focus from traditional handcrafted data structures [17–24] to learnable neural alternatives in the domain of graph stream summarization. These neural structures seek to harness flexible, neural-driven compression mechanisms to attain superior compression ratios. We summarize their main advantages as follows: first, the adaptive allocation of greater memory resources to salient information; and second, the utilization of global contextual insights to dynamically reconfigure storage layouts.

However, applying neural networks to graph stream summarization remains a challenging endeavor. The fundamental challenge lies in effectively compressing the massive, unbounded information of high-velocity graph streams into strictly constrained memory spaces while preserving the fidelity of edge weights.

To date, the pioneering work, Mayfly [25], has demonstrated the potential of neural networks to surpass traditional handcrafted sketches. It introduces a memory-augmented network with bounded gradients, leveraging a pre-training followed by fine-tuning paradigm to achieve accuracy comparable to or exceeding that of handcrafted sketches across datasets of varying scales. Mayfly further incorporates hash-based sharding to enable manual expansion of memory capacity at the onset of a task. Additionally, several designs for neural networks in general data streams offer valuable insights. For instance, MetaSketch [26] establishes a meta-learning framework on synthetic data for general item frequency estimation in data streams, while its successor LegoSketch [27] extends by introducing a modular architecture of memory bricks for more flexible adaptation to dynamic budgets.

Nevertheless, these approaches encounter critical limitations. **First and foremost**, they lack mechanisms to differentiate and isolate items based on frequency, a necessity highlighted in traditional sketch literature [28, 29]. Real-world graph streams typically exhibit highly skewed distributions, where a small number of frequent items coexist with a vast number of infrequent items. In existing neural architectures, when these diverse items are co-located within the same memory address space, the dominant updates from frequent items inevitably overshadow the subtle signals of infrequent ones. Our empirical observations confirm that this leads to severe overestimation of infrequent items. This issue becomes particularly pronounced in neural contexts: while neural networks can effectively resolve collisions among items of similar magnitude, they

remain ineffective against the mixture of frequent and infrequent items. Fundamentally, this is because existing encoding networks lack contextual awareness and fail to estimate stream frequencies explicitly. Lacking this discrimination, the subsequent calibration network is unable to disentangle the subtle features of infrequent items from the overwhelming signals of frequent items, thereby failing to recover the fidelity of the more vast number of infrequent items. **Second**, the reliance on hash-based sharding for memory management necessitates manual configuration at task initiation. This static allocation strategy is ill-suited for real-world scenarios where stream volumes escalate continuously, preventing the system from adapting dynamically to growing storage demands.

1.2 Our Proposed Solution

To address these challenges, we introduce **Crane**, a hierarchical neural architecture designed for robust graph stream summarization. Unlike flat structures that force all items into a single shared space, Crane organizes memory into a stack of layers and employs a **hierarchical carry mechanism** to physically segregate items based on their magnitude. This design directly counters the interference problem: by automatically lifting frequent items to higher layers, Crane ensures they do not monopolize the limited capacity reserved for infrequent items in lower layers.

Functionally, Crane operates through a streamlined workflow consisting of **Store** and **Query** phases. During the Store phase, a lightweight **encoding network** first maps each incoming edge to a two-dimensional basis matrix. Instead of static accumulation, the insertion follows a bottom-up trajectory governed by our proposed **hierarchical carry mechanism**. Specifically, the system performs an on-the-fly estimation at the current layer; if the estimated frequency exceeds a learned threshold, the excess mass is "carried" (promoted) to the subsequent layer. This process dynamically disentangles the traffic: recurring patterns migrate to upper layers like arithmetic carries, while sporadic interactions remain at the bottom. During the **Query** phase, Crane retrieves partial estimates from all active layers and aggregates them via a learnable linear decoder to produce the final high-fidelity frequency.

Furthermore, this hierarchical workflow inherently enables **smooth automatic memory expansion**. In contrast to hash-based sharding which requires pre-allocating fixed buckets, Crane monitors the saturation of the top-most layer during the Store phase. New upper layers are dynamically allocated only when the current hierarchy is saturated. This allows the memory footprint to grow logarithmically with stream volume, optimizing resource utilization in unbounded stream scenarios. Experimental results demonstrate that Crane reduces the Average Relative Error (ARE) by at least 10 \times compared to state-of-the-art methods.

Our contributions can be summarized as follows:

- We propose Crane, a hierarchical neural architecture for graph stream summarization that automatically segregates frequent and infrequent items via a hierarchical carry mechanism.
- We further introduce a smooth automatic memory expansion mechanism to adapt to real-world scenarios with continuously expanding network traffic, while reducing the memory space complexity from linear to logarithmic.

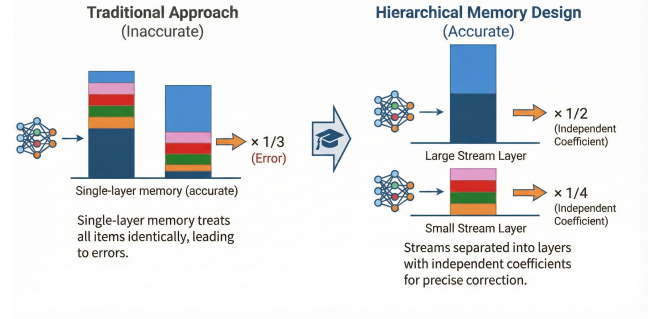


Figure 1: Overview of the motivating example.

- Experimental results demonstrate that Crane reduces Average Relative Error (ARE) by roughly 10 \times compared to state-of-the-art (SOTA) methods under identical memory constraints.

2 RELATED WORK

Graph stream summarization has attracted considerable research attention in recent years. We categorize existing methods into hand-crafted structures and neural structures.

2.1 Handcrafted Structures

Handcrafted graph stream summarization methods primarily focus on achieving accurate estimates under relatively abundant memory conditions, subsequently extending their accuracy to scenarios with limited memory. Notable approaches in this domain include TCM [18], GSS [19, 21], and Auxo [24]. TCM [18] extends the idea of the Count-Min Sketch (CMS) [30]¹ by leveraging a pre-defined $m \times m$ compressed matrix M to store graph stream items, where it employs a hash function $h(\cdot)$ with range $[0, m]$ to map an item to a corresponding bucket in M . For an incoming edge $s_i \rightarrow d_i$, TCM adds its associated weight w_i to the value in bucket $M[h(s_i), h(d_i)]$, merging nodes with the same hash value. This supports boolean queries (e.g., edge existence) and aggregation queries (e.g., summing weights in the $h(x)$ -th column for outgoing edges from x). However, TCM suffers from poor query accuracy due to hashing collisions.

To improve accuracy, GSS [19, 21] incorporates a f -bit fingerprint ξ_v (a hash value) for each node v alongside the weight in the compressed matrix. GSS comprises a $m \times m$ matrix M and an adjacency list as an extra buffer. Upon inserting an item $e_i = (\langle s_i, d_i \rangle; w_i; t_i)$, GSS computes fingerprints $\langle \xi_{s_i}, \xi_{d_i} \rangle$ and stores them with w_i in $M[h(s_i), h(d_i)]$. If edges with different fingerprint pairs collide, the newcomer is stored in the buffer. To minimize buffer size, GSS uses square hashing to generate multiple candidate buckets $\{M[h_j(s_i), h_j(d_i)] \mid 1 \leq j \leq r, 1 \leq j \leq r\}$ for each edge, recording $\langle \xi_{s_i}, \xi_{d_i}, w_i, \text{idx}_{\text{pair}} \rangle$ in an empty candidate, where idx_{pair} denotes the indices. The leftover edges go to the buffer. For large-scale streams, the growing buffer incurs high memory and insertion costs. Auxo [24] addresses scalability issues in prior designs by proposing a prefix-embedded tree (PET) that extends building blocks in a

¹CMS is a probabilistic data structure for estimating item frequencies in one-dimensional data streams. It uses d arrays, each with w counters and an associated hash function. On an item's arrival, it increments the hashed counter in each array by 1, and a query returns the minimum of these d counters to minimize over-estimation. Its variants include the Count Sketch [31], the Conservative Update Sketch [32], etc.

tree-style manner, achieving logarithmic insert/query times and reducing storage by a scale $\log |E|$, where $|E|$ is the edge set size. PET embeds binary prefixes into the tree, omitting i -bit prefixes on level i . To enhance memory utilization, Auxo introduces a proportional PET that expands levels incrementally. However, these methods lack explicit accuracy correction mechanisms, limiting adaptability under severe memory constraints.

2.2 Neural Structures

Neural graph stream summarization methods focus on recovering precise estimates under severe memory constraints using neural networks. The pioneering method Mayfly [25] introduces the first neural data structure specifically for graph stream summarization, surpassing handcrafted solutions like TCM and GSS by leveraging memory-augmented neural networks (MANNs) [33, 34] and one-shot meta-learning. Mayfly is trained in two offline phases: the larval phase, where it acquires fundamental summarization abilities from larval meta-tasks generated using synthetic data to promote generalization across distributions; and the metamorphosis phase, where it rapidly adapts to real graph streams via metamorphosis meta-tasks sampled from target data, enhancing specialization. Architecturally, Mayfly employs a novel joint storage paradigm that separately compresses node and edge weights within a shared memory module to preserve graph structural information, enabling efficient one-pass processing. It incorporates information pathways—configurable routes through the network that guide data flow during meta-learning—to support diverse graph queries without retraining, including edge queries (e.g., estimating edge weights), node queries (e.g., node degrees), connectivity queries (e.g., reachability), path queries (e.g., shortest path approximations), and subgraph queries (e.g., motif counting). This design mitigates issues like hash collisions in low-budget scenarios and achieves superior accuracy by exploiting deep implicit features.

Related neural data stream structures, while not graph-specific, offer insights for graph applications. MetaSketch [26] is a neural sketch for general item frequency estimation, using meta-learning on synthetic Zipf-distributed meta-tasks in a pre-training phase, with basic and advanced versions that adapt to skewed real streams via online sampling, outperforming traditional sketches through differentiable encoding/decoding. LegoSketch [27], a scalable MANN for data stream sketching, coordinates multiple memory bricks for dynamic adaptation to varying space budgets and domains, incorporating normalized multi-hash embedding for domain-agnostic scalability, self-guided weighting loss for meta-task optimization, and memory scanning for feature reconstruction, achieving better space-accuracy trade-offs. However, they share two common issues: 1) lack of contextual optimization for memory management, limiting compression; 2) hash-based sharding for memory expansion struggles with continuously growing data volumes.

3 CRANE DESIGN

3.1 Overview

At an operational level, Crane adheres to the fundamental **Store** and **Query** paradigm characteristic of graph stream summarization. However, distinct from traditional flat architectures, Crane introduces three synergistic innovations to maximize estimation

fidelity and enable dynamic scalability: **Hierarchical Memory**, **Learnable Encoder–Decoder**, and **Hierarchical Carry Mechanism**, as illustrated in Figure 2. By integrating these components into the standard workflow, Crane transforms the static sketching process into a dynamic, hierarchical one. Specifically, the learnable encoder–decoder maps edges into a multi-layered memory structure, while the hierarchical carry mechanism automatically governs the vertical flow of information. Together, these designs allow Crane to physically isolate high-frequency items from low-frequency noise and achieve smooth, automatic memory expansion as the stream volume grows.

In the remainder of this section, we detail the implementation of these components. We first present the design of the learnable encoder–decoder and its interaction with the hierarchical memory in § 3.2. We then demonstrate how the hierarchical carry mechanism effectively separates large and small items across layers in § 3.3. Next, we explain how this carry mechanism unlocks the smooth automatic expansion capability in § 3.4. Finally, we describe the training strategy based on purely synthetic data in § 3.5, ensuring robust generalization to real-world graph streams.

3.2 Hierarchical Learnable Memory

As shown in Figure 3, Crane realizes hierarchical learnable hashing by assigning a distinct neural encoder $f_i(\cdot)$ to each memory layer $i \in \{1, \dots, N\}$. These encoders implement differentiable hash functions that map discrete edge identifiers to continuous basis matrices. Using different encoders across layers allows the model to redistribute and progressively disentangle collisions: higher layers can selectively preserve or cancel conflicts that arise in lower layers, rather than inheriting them rigidly.

3.2.1 Store path. Prior neural data structures such as Mayfly and Lego Sketch employ carefully engineered binary encodings and complex transformation pipelines (e.g., multi-stage representation modules, sparse attention, or normalized multi-hash embeddings) to couple traditional hashing with neural mappings. However, these complex transformation pipelines introduce highly non-linear optimization landscapes. We argue that for graph streams, the core inductive bias lies in the structural coupling between source and destination nodes. Consequently, Crane adopts a minimal design based on MLPs and an outer-product operation, which both reduces model complexity and matches the two-dimensional query structure of point lookups in graph streams.

As illustrated in the encoding branch of Figure 2, Crane treats each edge not as a point, but as a two-dimensional signal pattern (a *basis matrix*). The store operation simply superimposes this unique pattern onto the shared memory surface via addition. This strategy distributes the edge’s information across the entire grid, allowing the neural encoders to naturally minimize interference through “soft” superposition rather than rigid hash collisions.

The formal procedure for this process is outlined in the **STORE** module of Algorithm 1. Specifically, given an input edge

$$e = (o_i, d_i, w_i), \quad (1)$$

we first obtain binary encodings B_{o_i} and B_{d_i} of the source and destination endpoints. Two independent encoders are then applied

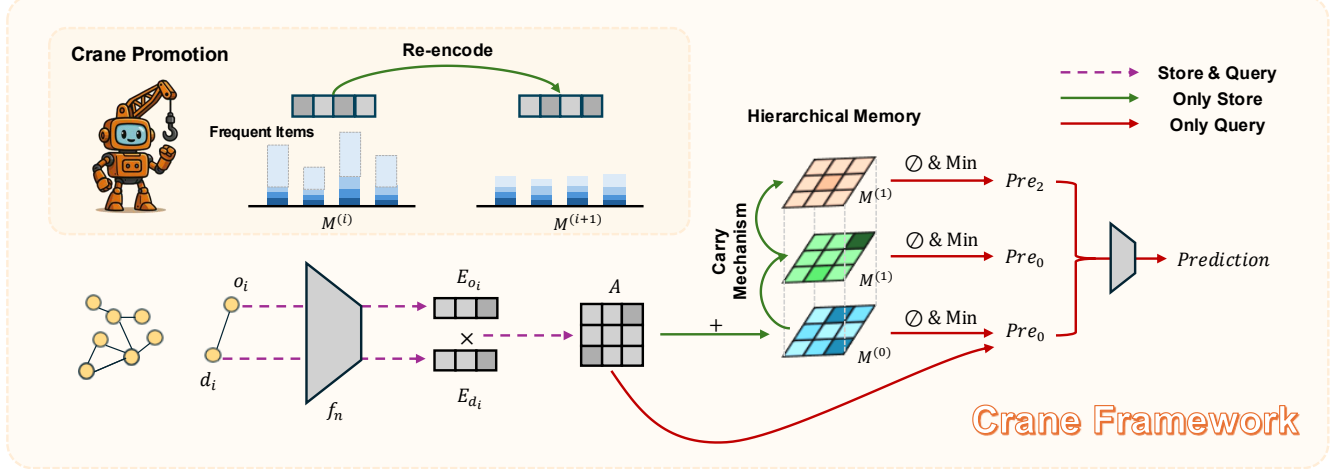


Figure 2: The overall architecture of Crane.

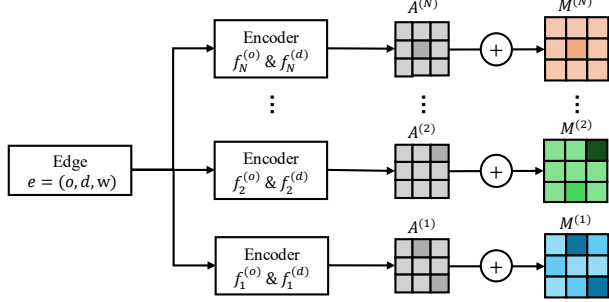


Figure 3: Hierarchical Learnable Memory.

to these encodings to obtain continuous embeddings:

$$\mathbf{E}_{o_i} = f^{(o)}(B_{o_i}), \quad \mathbf{E}_{d_i} = f^{(d)}(B_{d_i}). \quad (2)$$

Both encoders use non-negative activation functions (e.g., ReLU), ensuring that the generated embeddings $\mathbf{E}_{o_i}, \mathbf{E}_{d_i} \in \mathbb{R}^{H \times W}$ are non-negative element-wise, where H and W denote the height and width of the encoding matrix, respectively. We construct a two-dimensional basis matrix $A \in \mathbb{R}^{H \times W}$ via the outer product:

$$A = \mathbf{E}_{o_i} \mathbf{E}_{d_i}^\top + \varepsilon, \quad (3)$$

where ε is a small positive constant added element-wise to avoid zero entries and stabilize subsequent division. Each layer maintains a memory matrix $M \in \mathbb{R}^{H \times W}$, which is initialized to zero. The write operation at a given layer simply accumulates this basis matrix into the corresponding memory M :

$$M \leftarrow M + w_i \cdot A. \quad (4)$$

3.2.2 Query path. Mayfly follows the Count-Min principle at query time by aggregating multiple memory positions and feeding a rich set of statistics (e.g., sums, maxima, minima, original node/edge encodings, and even the total item count) into a decode network. Analytically, feeding such a heterogeneous set of statistics introduces two fundamental issues. First, including the total item count predisposes the model to *shortcut learning*: the decoder tends to overfit to the global stream magnitude rather than learning to resolve local hash collisions. This dependency explains the training

instability observed when global signals are removed, as the gradients lose their primary (albeit coarse) guide. Second, sum-based pooling aggregates collision noise from all buckets, inherently suffering from a low Signal-to-Noise Ratio (SNR) compared to the minimum statistic, which offers the tightest upper bound in Count-Min logic. Incorporating these noisy signals dilutes the information density and forces the decoder to filter out irrelevant background variance.

Crane deliberately avoids these redundant paths. Instead, we use the most informative statistic for Count-Min style decoding—the minimum of the ratio between memory and basis matrix—as the *only* input to the decoder, thus providing a clear and stable supervisory signal.

Retrieving the frequency follows the inverse flow shown in Figure 2. We first regenerate the target edge’s basis pattern and compare it element-wise against the accumulated memory. Since the memory is a sum of non-negative signals, the ratio between the memory and the basis at any position gives a candidate frequency estimate (an upper bound). By taking the minimum of these ratios, Crane rigorously filters out the noise contributed by other overlapping edges, recovering estimate. The formal insertion procedure is detailed in the Query operation of Algorithm 1.

We provide the step-by-step pseudocode in Algorithm 1 and detail its mathematical formulation below. Given a memory M and a basis matrix A constructed for the query edge, we define

$$Q(M, A) = \min(M \oslash A) \quad (5)$$

where \oslash denotes element-wise division and the minimum is taken over all positions. This scalar $Q(M, A)$ serves as the per-layer estimate produced by Count-Min style decoding.

3.2.3 Multi-layer decoding. In the hierarchical setting, each layer i maintains its own memory $M^{(i)}$ and encoder, yielding a per-layer basis matrix $A^{(i)}$ and estimate

$$q_i(e) = Q(M^{(i)}, A^{(i)}). \quad (6)$$

We collect these into a vector

$$\mathbf{q}(e) = [q_1(e), q_2(e), \dots, q_N(e)]^\top. \quad (7)$$

Algorithm 1 Store and Query Operations

```

1: Data: Edge  $e = (o_i, d_i, w_i)$ ; number of layers  $N$ ; layer-specific encoders  $\{f_i^{(o)}, f_i^{(d)}\}_{i=1}^N$ ; memories  $\{M^{(i)} \in \mathbb{R}^{H \times W}\}_{i=1}^N$ ; decoder parameters  $\mathbf{w} \in \mathbb{R}^N, b \in \mathbb{R}$ .
2: Operation STORE( $e$ ):
3:  $B_{o_i} \leftarrow \text{BINARYENCODE}(o_i); B_{d_i} \leftarrow \text{BINARYENCODE}(d_i)$ 
4: for  $i \leftarrow 1$  to  $N$  do
5:    $\mathbf{E}_{o_i}^{(i)} \leftarrow f_i^{(o)}(B_{o_i}); \mathbf{E}_{d_i}^{(i)} \leftarrow f_i^{(d)}(B_{d_i})$ 
6:    $\mathbf{E}_{o_i}^{(i)}, \mathbf{E}_{d_i}^{(i)} \leftarrow \max(\mathbf{E}_{o_i}^{(i)}, 0), \max(\mathbf{E}_{d_i}^{(i)}, 0)$ 
7:    $A^{(i)} \leftarrow \mathbf{E}_{o_i}^{(i)}(\mathbf{E}_{d_i}^{(i)})^\top + \epsilon$ 
8:    $M^{(i)} \leftarrow M^{(i)} + w_i \cdot A^{(i)}$ 
9: end for

10: Operation QUERY( $e$ ):
11:  $B_{o_i} \leftarrow \text{BINARYENCODE}(o_i); B_{d_i} \leftarrow \text{BINARYENCODE}(d_i)$ 
12: for  $i \leftarrow 1$  to  $N$  do
13:    $\mathbf{E}_{o_i}^{(i)} \leftarrow f_i^{(o)}(B_{o_i}); \mathbf{E}_{d_i}^{(i)} \leftarrow f_i^{(d)}(B_{d_i})$ 
14:    $A^{(i)} \leftarrow \mathbf{E}_{o_i}^{(i)}(\mathbf{E}_{d_i}^{(i)})^\top + \epsilon$ 
15:    $R^{(i)} \leftarrow M^{(i)} \oslash A^{(i)}$ 
16:    $q_i(e) \leftarrow \min_{p,q} R_{pq}^{(i)}$ 
17: end for
18:  $\mathbf{q}(e) \leftarrow [q_1(e), \dots, q_N(e)]^\top$ 
19: return  $\hat{y}(e) \leftarrow \mathbf{w}^\top \mathbf{q}(e) + b$ 

```

Crane then employs a single linear regression layer as a learnable decoder to aggregate layer-wise estimates into the final prediction:

$$\hat{y}(e) = \mathbf{w}^\top \mathbf{q}(e) + b, \quad (8)$$

where $\mathbf{w} \in \mathbb{R}^N$ and $b \in \mathbb{R}$ are trainable parameters. This decoder is intentionally lightweight, so that the modeling capacity is primarily devoted to the encoders and the hierarchical memory itself.

3.3 Hierarchical Carry Mechanism

When large and small items are stored in the same memory cells, the neural decoder must infer a large dynamic range from heavily entangled signals, which is intrinsically difficult. A natural remedy is to separate items of different magnitudes across layers. However, realizing such a separation faces two key challenges. First, mainstream sketching methods—both neural and hand-crafted—perform context-free updates, so they cannot directly access an estimate of the current items size during insertion. Second, modifying the encoding as a function of observed counts may break consistency between past and future encodings and complicate decoding.

Crane addresses both challenges with a hierarchical carry mechanism inspired by positional numeral systems. During each write, we perform an inexpensive local query to obtain a current estimate of the edge frequency and, if necessary, promote part of its mass to the next layer. Because we reuse the same encoding for both local query and promotion, encoding consistency is preserved.

Figure 4 (Left) charts this bottom-up promotion flow. After updating the current layer $M^{(i)}$, Crane immediately queries the edge’s local estimate $Q(M^{(i)}, A^{(i)})$. As shown by the decision branches, if this estimate exceeds the threshold θ , the overflow is “carried”

upward to layer $i + 1$; otherwise, the process terminates. This conditional logic, formalized in Algorithm 2, effectively acts as a sieve, filtering heavy hitters from the noise below.

Consider an edge e and its basis matrix $A^{(i)}$ at layer i with memory $M^{(i)}$. We first obtain an estimate of its frequency at this layer:

$$\hat{y}_i(e) = Q(M^{(i)}, A^{(i)}). \quad (9)$$

Let $\theta > 0$ be a user-specified carry threshold. We define an integer carry factor

$$T_e^{(i)} = \left\lfloor \frac{\hat{y}_i(e)}{\theta} \right\rfloor_+, \quad (10)$$

where $\lfloor \cdot \rfloor_+$ denotes rounding down and clipping to non-negative integers. If $T_e > 0$, we apply a carry operation:

$$M^{(i+1)} \leftarrow M^{(i+1)} + T_e^{(i)} \cdot A^{(i)}, \quad (11)$$

$$M^{(i)} \leftarrow M^{(i)} - \theta T_e^{(i)} \cdot A^{(i)}. \quad (12)$$

Intuitively, items whose estimated count exceeds θ are partially promoted to the next layer, while their contribution in the current layer is reduced proportionally. Collisions may be carried upwards together with large items, but thanks to the layer-specific encoders introduced in §3.2, the higher layer can selectively preserve or resolve these collisions.

3.3.1 Mini-batch conservative carry. A straightforward implementation that processes edges strictly sequentially yields the most accurate carry decisions, but severely limits parallelism: the carry factor T_e for each edge depends on the exact sequence of prior updates and conflicts. Batch processing introduces a tension between correctness and efficiency. A naive conservative strategy that carries at most once per conflicting cell can significantly under-promote large items, while an aggressive strategy that treats every conflict as a carry candidate may violate the non-negativity of memory entries.

To improve parallelism with minimal accuracy loss, Crane adopts a mini-batch conservative carry scheme. We process edges in mini-batches B and perform carries only when the current batch-wise estimate clearly exceeds the threshold.

Let A_e denote the basis matrix generated for a single edge e . For a mini-batch of edges B , we compute the aggregated basis matrix A_B and update the memory as follows:

$$A_B^{(i)} = \sum_{e \in B} A_e^{(i)}, \quad (13)$$

$$M^{(i)} \leftarrow M^{(i)} + A_B^{(i)}. \quad (14)$$

We then compute, for each edge $e \in B$, a conservative binary carry indicator

$$T_B^{(i)} = \left\lfloor \frac{Q(M^{(i)}, A_B^{(i)})}{\theta} \right\rfloor_+, \quad (15)$$

and update the adjacent layers as

$$M^{(i+1)} \leftarrow M^{(i+1)} + T_B^{(i)} \cdot A_B^{(i)}, \quad (16)$$

$$M^{(i)} \leftarrow M^{(i)} - \theta T_B^{(i)} \cdot A_B^{(i)}. \quad (17)$$

Each edge is thus promoted at most once per mini-batch, which corresponds to a conservative approximation of the fully sequential

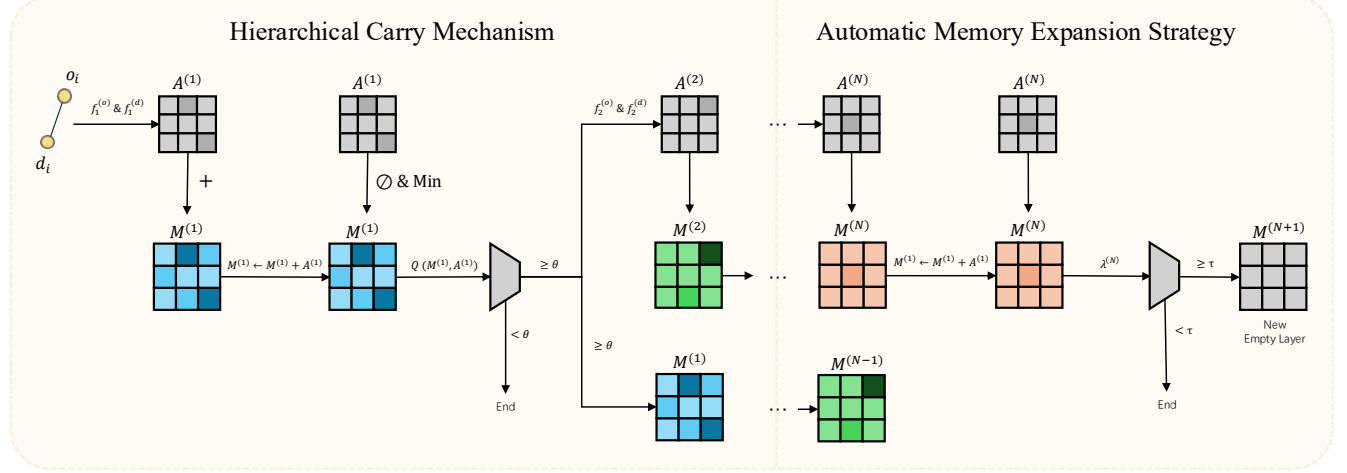


Figure 4: Hierarchical Carry Mechanism and Automatic Memory Expansion Strategy.

Algorithm 2 Hierarchical Carry Mechanism: Sequential vs. Mini-batch

```

1: Data: Layer index  $i$ ; memories  $M^{(i)}, M^{(i+1)}$ ; carry threshold  $\theta > 0$ ;
   stream of edges  $\mathcal{S}$  with basis matrices  $\{A_e^{(i)}\}$ .
2: Module SequentialCarry( $\mathcal{S}, i$ ):
3: for edge  $e \in \mathcal{S}$  in arrival order do
4:    $q_i(e) \leftarrow Q(M^{(i)}, A_e^{(i)})$ 
5:    $T_e^{(i)} \leftarrow \lfloor q_i(e) / \theta \rfloor_+$ 
6:   if  $T_e > 0$  then
7:      $M^{(i+1)} \leftarrow M^{(i+1)} + T_e^{(i)} \cdot A_e^{(i)}$ 
8:      $M^{(i)} \leftarrow M^{(i)} - \theta T_e^{(i+1)} \cdot A_e^{(i)}$ 
9:   end if
10: end for
11: Module MiniBatchConservativeCarry( $\mathcal{S}, i$ ):
12: Partition  $\mathcal{S}$  into mini-batches  $\{B_1, B_2, \dots\}$ 
13: for mini-batch  $B$  do
14:    $A_B^{(i)} \leftarrow \sum_{e \in B} A_e^{(i)}$ 
15:    $M^{(i)} \leftarrow M^{(i)} + A_B^{(i)}$ 
16:    $q_i^B \leftarrow Q(M^{(i)}, A_B^{(i)})$ 
17:    $T_B \leftarrow \lfloor q_i^B / \theta \rfloor_+$ 
18:   if  $T_B > 0$  then
19:      $M^{(i+1)} \leftarrow M^{(i+1)} + T_B^{(i)} \cdot A_B^{(i)}$ 
20:      $M^{(i)} \leftarrow M^{(i)} - \theta T_B^{(i+1)} \cdot A_B^{(i)}$ 
21:   end if
22: end for

```

process. Empirically, this mini-batch carry mechanism substantially improves parallel efficiency while having negligible impact on estimation accuracy.

3.4 Automatic Memory Expansion Strategy

Since the hierarchical carry mechanism repeatedly promotes large items to higher layers, Crane naturally supports smooth, automatic expansion and can therefore operate in settings where the total number of edges is unknown in advance.

Prior work such as Mayfly uses hash-based sharding: a heavy stream is split into multiple substreams, each stored in an independent sketch, in order to reduce collisions and ease the burden on the neural decoder. In contrast, Crane relies on vertical separation across layers. The hierarchical carry mechanism continually lifts frequent items from lower to higher layers and, in principle, does not impose a hard upper bound on the number of layers. This property gives Crane a natural path to smooth automatic expansion and makes it well-suited to scenarios with unknown or highly variable stream sizes.

Figure 4 (Right) illustrates this elastic growth. Crane continuously monitors the saturation of the topmost layer $M^{(N)}$. Once the load surpasses a safety margin, the system triggers the creation of a “New Empty Layer” $M^{(N+1)}$ atop the stack, as depicted. This mechanism, detailed in Algorithm 3, allows the memory hierarchy to expand organically with the stream volume, avoiding the need for pre-allocation.

During training, we allocate a maximum number of layers N_{\max} and generate synthetic streams such that the highest layer is frequently activated, exposing the model to the full spectrum of promotion behaviors. At inference time, we start with a small number of layers and expand the hierarchy only when necessary. Let the current top layer be indexed by L with memory matrix $M^{(L)} \in \mathbb{R}^{H \times W}$. We define a simple utilization indicator for the top layer as the average mass per cell:

$$\lambda^{(L)} = \frac{1}{HW} \sum_{p=1}^H \sum_{q=1}^W M_{pq}^{(L)}. \quad (18)$$

Given a user-specified load threshold $\tau > 0$ and an upper bound N_{\max} on the number of layers, Crane expands the memory hierarchy according to

$$\text{if } \lambda^{(L)} > \tau \text{ and } L < N_{\max}, \text{ then add a new layer } M^{(L+1)} \leftarrow \mathbf{0}. \quad (19)$$

We then continue processing the stream with the enlarged hierarchy. Subsequent carry operations automatically transfer mass into the newly added layer without any change to the insertion or query interfaces.

Algorithm 3 Automatic Memory Expansion

```

1: Data: Current number of layers  $L$ ; memories  $\{M^{(i)} \in \mathbb{R}^{H \times W}\}_{i=1}^L$ ;
   maximum allowed layers  $N_{\max}$ ; load threshold  $\tau > 0$ .
2: Output: Updated number of layers  $L$  and memories.
3:  $M^{(L)}$  is the current top-layer memory
4:  $\lambda^{(L)} \leftarrow \frac{1}{HW} \sum_{p=1}^H \sum_{q=1}^W M_{pq}^{(L)}$ 
5: if  $\lambda^{(L)} > \tau$  and  $L < N_{\max}$  then
6:    $L \leftarrow L + 1$ 
7:    $M^{(L)} \leftarrow \mathbf{0}^{H \times W}$ 
8: end if
9: return  $\{M^{(i)}\}_{i=1}^L, L$ 

```

This strategy allows memory usage to grow only when the sketch is genuinely saturated and, in practice, roughly logarithmically with respect to the stream volume. Consequently, Crane adapts its footprint to the difficulty and scale of the workload, while avoiding expensive reconfiguration or retraining. In particular, when a single machine monitors multiple streams simultaneously, Crane can automatically allocate more layers—and therefore more memory—to heavier streams, while keeping the footprint of lighter streams small. This per-stream elasticity improves overall memory utilization and simplifies deployment, since operators no longer need to predict stream sizes or manually tune sketch capacities in advance.

3.5 Training

Crane is trained entirely offline on synthetic graph streams and is then directly evaluated on real workloads without any additional fine-tuning. Our training strategy follows the meta-task view used in prior neural sketches for graph streams, where each synthetic stream together with its ground-truth queries forms a single task.² Unlike Mayfly, we do not introduce a separate adaptation phase on real graph streams, and all parameters of the encoders, hierarchical memory, carry mechanism, and decoder are shared across tasks and datasets.

3.5.1 Task formulation. Each training task t simulates storing and querying a single graph stream instance. Formally, task t consists of a support set S_t and a query set Q_t . The support set

$$S_t = \{x_1^{(t)}, x_2^{(t)}, \dots, x_{L_t}^{(t)}\}$$

is a sequence of streaming edges $x_\ell^{(t)} = (o_\ell, d_\ell, w_\ell)$, which are fed to the STORE operation (Algorithm 1) in arrival order. The query set

$$Q_t = \{(e_j^{(t)}, y_j^{(t)})\}_j$$

contains a subset of edges $e_j^{(t)} = (o_j, d_j)$ together with their exact cumulative frequencies

$$y_j^{(t)} = \sum_{\ell: (o_\ell, d_\ell) = (o_j, d_j)} w_\ell$$

computed from the full support stream S_t . During training, we reset the hierarchical memories $\{M^{(i)}\}$ at the beginning of each task, run STORE on S_t once, and then apply QUERY to all edges in Q_t to obtain predictions $\hat{y}_j^{(t)}$.

²Conceptually similar to the larval pre-training phase of Mayfly [25].

3.5.2 Synthetic graph-stream generation. To endow Crane with general summarization ability instead of memorizing specific datasets, all tasks are generated from synthetic graph streams, following the practice of Mayfly’s larval tasks [25]. We use a unified numerical ID space for nodes (e.g., integers mapped to fixed-length binary codes), so the encoders in §3.2 are trained in a domain-agnostic manner and can be reused on real streams without retraining.

For each task t , we construct a synthetic stream S_t in three steps. First, we sample a stream length L_t from a range $[1, \Gamma]$ and generate endpoints (o_ℓ, d_ℓ) by drawing node IDs independently from the global ID space. This produces diverse graph structures and collision patterns within the sketch. Second, we sample a Zipf distribution $\text{Zipf}(\alpha_t)$ from a pool of exponents $\alpha_t \in [\alpha_{\min}, \alpha_{\max}]$, reflecting the skewed edge-weight distributions commonly observed in real graphs. We then generate a normalized weight profile $\{\tilde{w}_\ell\}_{\ell=1}^{L_t}$ by i.i.d. sampling from $\text{Zipf}(\alpha_t)$ and rescaling so that $\sum_\ell \tilde{w}_\ell = 1$. Finally, we draw a total weight W_t from a log-uniform range and set $w_\ell = W_t \tilde{w}_\ell$ for each edge. The query set Q_t consists of all distinct edges in S_t , together with their exact cumulative weights $\{y_j^{(t)}\}$ computed by aggregation.

This construction exposes Crane to a wide spectrum of stream lengths, skewness levels, and frequency scales during training, and naturally exercises the carry mechanism and automatic expansion mechanisms described in §3.3 and §3.4.

3.5.3 Loss function. Edge frequencies in graph streams typically follow a heavy-tailed distribution, spanning several orders of magnitude. To ensure robust optimization across this wide dynamic range, we adopt the Mean Absolute Error (MAE) as our training objective. Unlike squared error metrics that can be overly sensitive to outliers (i.e., extremely frequent edges), the L_1 loss provides a stable gradient signal that encourages accurate estimation for both heavy hitters and tail items.

Formally, given a task t and its query set Q_t , the loss is defined as:

$$\mathcal{L}_t = \frac{1}{|Q_t|} \sum_{(e_j^{(t)}, y_j^{(t)}) \in Q_t} \left| y_j^{(t)} - \hat{y}_j^{(t)} \right|, \quad (20)$$

where $\hat{y}_j^{(t)}$ denotes the frequency predicted by the decoder, and $y_j^{(t)}$ is the ground-truth cumulative weight. Minimizing this objective directly aligns the model’s predictions with the true counts, ensuring that the learnable components—encoders, memory, and decoder—converge to a state that accurately preserves the stream statistics.

3.5.4 Optimization. We train Crane by sampling mini-batches of tasks $\{t\}$ on the fly and minimizing the average task loss $\mathcal{L} = \frac{1}{B} \sum_{t=1}^B \mathcal{L}_t$ with AdamW [35]. Within each task, edges are processed in mini-batches of streaming updates so that the mini-batch conservative carry mechanism in Algorithm 2 can be applied efficiently. All learnable parameters, including the encoder networks for each layer, the linear decoder, and the shared promotion and expansion thresholds, are optimized jointly. Training uses only synthetic tasks; at evaluation time, we fix all parameters and run Crane in a purely streaming fashion on real graph streams, with no gradient updates and no dataset-specific tuning.

4 MATHEMATICAL ANALYSIS

In this section, we provide a theoretical analysis of Crane's performance characteristics. We establish four key properties: logarithmic efficiency in both space and time, exponential decay of collision probability, and minimized error variance.

4.1 Preliminaries and Assumptions

Let \mathcal{S} be a graph stream of edge updates. Let $f(e)$ denote the true frequency of an edge e . Crane maintains a hierarchy of N memory layers $\{M^{(1)}, \dots, M^{(N)}\}$ with a promotion threshold $\theta > 1$.

- **Assumption 1 (Independent Hashing).** The neural encoders $f_i(\cdot)$ act as pairwise independent hash functions. For distinct edges e_i, e_j , the collision probability at layer l is bounded by a small constant $p \in (0, 1)$, independent across layers.
- **Assumption 2 (Noise Distribution).** The value stored in a memory cell is $X_l = \text{signal}_l(e) + \epsilon_l$, where $\epsilon_l \geq 0$ represents non-negative additive collision noise.

4.2 Complexity Analysis

We first address the computational efficiency of Crane. Unlike traditional sketches that often require linear memory expansion to handle heavy traffic, Crane utilizes a hierarchical carry-like mechanism to achieve logarithmic scaling in both space and time.

LEMMA 1 (LOGARITHMIC SPACE EFFICIENCY). *Given a promotion threshold θ , the number of layers L required to accurately represent an edge with maximum frequency F_{\max} grows logarithmically, specifically $L \geq \log_{\theta}(F_{\max} + 1)$. Consequently, the total space complexity relative to the stream volume is logarithmic.*

PROOF. See Appendix A.1. \square

THEOREM 2 (LOGARITHMIC AMORTIZED TIME COMPLEXITY). *Let \mathcal{S} be a stream of N edges with total accumulated weight W_{total} . The total time complexity to process \mathcal{S} is $O(N \log_{\theta} W_{\text{total}})$, and the amortized time complexity per insertion is $O(\log_{\theta} W_{\text{total}})$.*

PROOF. See Appendix A.2. \square

4.3 Error Bound Analysis

We now analyze the error bounds, demonstrating how Crane's hierarchical structure and learnable components minimize collision interference.

THEOREM 3 (EXPONENTIAL DECAY OF COLLISION PROBABILITY). *Under Assumption 1, the probability that a heavy hitter edge e suffers from consistent collision interference across all active layers decreases exponentially with the number of layers. Specifically, the joint collision probability across k layers is bounded by p^k .*

PROOF. See Appendix A.3. \square

THEOREM 4 (RESIDUAL ERROR BOUND). *Let $W_{\text{res}} = \sum_e (f(e) \pmod{\theta})$ be the residual weight retained in the bottom layer, and w be the width of the sketch. Assuming the convergence condition $p \cdot \theta < 1$, the expected estimation error is dominated by the bottom layer:*

$$E[\text{Error}_{\text{Crane}}] \approx O\left(\frac{W_{\text{res}}}{w}\right) \quad (21)$$

Since $W_{\text{res}} \ll \|\mathbf{f}\|_1$, Crane achieves a significantly tighter error bound than standard Count-Min Sketches.

PROOF. See Appendix A.4. \square

4.4 Optimization Properties

Learnable Orthogonality. For the set of heavy hitters, the gradient descent update rule drives the encoder parameters ϕ to minimize the inner product of basis matrices $\langle A_u, A_v \rangle$. Consequently, the effective collision probability for learned encoders satisfies $p_{\text{learn}} < p_{\text{random}}$ (See Appendix A.5 for derivation).

THEOREM 5 (VARIANCE MINIMIZATION VIA LINEAR DECODING). *The learnable linear decoder $\hat{y} = \sum w_l q_l + b$ yields an estimator with variance no greater than that of a fixed-weight decoder. It effectively acts as an Inverse-Variance Weighting mechanism, assigning lower weights to noisy lower layers.*

PROOF. See Appendix A.6. \square

4.5 Comparative Analysis: Hierarchical vs. Flat Structures

Finally, we provide a theoretical comparison between Crane and Mayfly [25], which map all updates into a single shared memory space M_{flat} . We demonstrate that Crane's hierarchical carry mechanism provides a structural guarantee for noise suppression that flat architectures lack.

THEOREM 6 (INTERFERENCE ISOLATION). *Let \mathcal{S} be a graph stream obeying a heavy-tailed distribution. Let $\text{Var}(\text{Noise}_{\text{Flat}})$ and $\text{Var}(\text{Noise}_{\text{Crane}})$ denote the variance of the collision noise affecting a target low-frequency edge e in a Flat Neural Sketch and Crane, respectively, under identical width w . Crane suppresses the collision noise by a factor proportional to the ratio of the residual weight to the total weight:*

$$\frac{\mathbb{E}[\text{Error}_{\text{Crane}}]}{\mathbb{E}[\text{Error}_{\text{Flat}}]} \approx \frac{W_{\text{res}}}{W_{\text{total}}} \ll 1 \quad (22)$$

where $W_{\text{total}} = \|\mathbf{f}\|_1$ and $W_{\text{res}} = \sum_e (f(e) \pmod{\theta})$.

PROOF. See Appendix A.7. \square

5 EVALUATION

Implementation and Environment. We implement *Crane* and make the source code publicly available for reproducibility. To ensure a comprehensive and fair comparison under strictly constrained memory budgets, we implement four baseline methods with specific adaptations:

- *Mayfly* [25], a pioneering neural graph stream summarization structure (for which we adopt the published Subimago configuration without additional fine-tuning on real data);
- *TCM* [18], a representative hash-based method that projects the graph stream onto a fixed-size adjacency matrix via hash functions [18], aggregating edge weights to maintain constant update time within bounded space.
- *GSS* [21], an accuracy-oriented sketch utilizing edge fingerprints and square hashing to mitigate collisions [21]. In our implementation, to adapt GSS to strict memory limitations, we compress the fingerprints and employ a binary search strategy to determine

Table 1: Accuracy Results (ARE) on Five Real-World Datasets under 64KB memory budget. The "Improv." row indicates the error reduction factor of Crane compared to the best baseline method.

Method	Lkml						NotreDame			
	20k	40k	80k	200k	400k	800k	200k	500k	1M	1.5M
TCM	1.61	3.31	6.48	17.52	34.40	67.60	38.01	96.23	194.56	292.02
GSS	6.35	10.69	67.68	44.11	292.08	574.10	54.64	128.68	253.90	378.63
Auxo	3.13	6.30	11.79	31.15	61.20	121.74	49.00	123.01	244.97	365.97
Mayfly	8.18	8.91	16.51	13.44	21.92	40.99	16.81	20.41	33.53	43.83
Crane	0.38	0.66	0.82	0.59	0.82	0.74	0.96	1.75	2.33	2.48
Improv.	4.24×	5.04×	7.92×	22.76×	26.75×	55.75×	17.50×	11.66×	14.41×	17.65×

Method	CAIDA				WiKiTalk				StackOverflow			
	2M	8M	16M	27.1M	2M	8M	16M	25.0M	2M	8M	16M	63.5M
TCM	78.38	329.14	677.37	1170.95	239.71	1200.56	2813.88	4863.01	382.46	1590.78	3280.84	12310.60
GSS	1169.30	4432.08	8398.45	13819.50	474.94	2137.63	4817.00	8047.13	1943.25	7793.01	15788.10	62121.12
Auxo	260.59	994.23	1961.88	3294.99	358.48	1498.17	3103.35	4952.20	471.28	1891.80	3793.29	13419.60
Mayfly	34.67	75.41	71.04	69.24	168.65	204.76	180.58	159.49	46.62	82.93	77.77	76.79
Crane	1.90	3.99	4.03	4.27	2.69	6.60	6.07	6.65	4.08	8.59	7.74	7.44
Improv.	18.22×	18.90×	17.61×	16.23×	62.63×	31.01×	29.75×	23.99×	11.44×	9.65×	10.04×	10.32×

the optimal fingerprint size that maximizes accuracy within the given memory budget.

- *Auxo* [24], a scalable structure leveraging a Prefix Embedded Tree (PET) for logarithmic update complexity [24]. Although originally designed for dynamic expansion, we constrain its memory footprint for fair comparison by similarly applying binary search to adjust the fingerprint compression ratio, finding the configuration that fits the memory limit while retaining the PET structure’s efficiency.

To evaluate performance under strict resource constraints, **we fix the memory budget to 64KB for all methods**. For *Crane*, *Auxo*, and *GSS*, which inherently support dynamic memory expansion, we explicitly enforce this 64KB cap as the hard upper limit during testing. All experiments are conducted on a server equipped with 8 NVIDIA RTX 5090 GPUs (32GB memory each), a 128-core Intel(R) Xeon(R) Gold 6459C CPU, and 720GB of RAM.

Datasets. We evaluate all methods on five widely used real-world graph stream datasets. For each dataset, we further construct subsets of different stream lengths by randomly sampling contiguous segments, as summarized in Table 1.

- *Lkml* [21, 25, 36] is an email-reply network from the Linux Kernel Mailing List, where each edge represents one user replying to another. We follow the stream construction in *Mayfly* [25] and treat time-ordered replies as a directed edge stream with unit weights.
- *CAIDA*³ is an IP flow dataset derived from the CAIDA 2018 UCSD Anonymized Internet Traces. We use one minute of traffic containing 27,121,713 packets and 850,200 distinct flows, where each flow is modeled as a directed edge between 32-bit encoded IPv4 addresses.

³http://www.caida.org/data/passive/passive_dataset.xml

- *WiKiTalk*⁴ is a user–user communication network built from Wikipedia talk pages, where an edge from u to v means that user u wrote a message on user v ’s talk page. We use the English subset from this collection, sort all interactions by their timestamps, and treat them as a directed edge stream. The resulting stream contains 24,981,163 edges and 9,379,561 distinct user pairs.

- *StackOverflow* [37]⁵ is a user-user interaction graph from the SNAP collection. Each temporal interaction (question, answer, or comment) is treated as a directed edge, and we process all edges in chronological order as a graph stream. The resulting stream contains 63,497,050 edges and 36,233,450 distinct user pairs.

- *NotreDame* [38]⁶ is a web graph from the nd.edu domain. Nodes are web pages and edges are hyperlinks; we generate a graph stream by taking a random permutation of all directed edges. In this dataset each edge appears exactly once, so it does not exhibit the repeated-updates pattern of typical graph streams. We mainly use it to evaluate how well different sketches handle hash collisions under a large number of distinct edges. The resulting stream comprises 1,497,134 directed edges, all of which are distinct, i.e., it contains 1,497,134 unique edges.

These datasets are standard benchmarks in graph stream summarization, covering IP networks, online Q&A forums, collaborative editing platforms, and web graphs.

Metrics. To quantify estimation accuracy, we employ two standard metrics: Average Absolute Error (AAE) and Average Relative Error (ARE). They are defined as:

$$AAE = \frac{1}{|Q|} \sum_{q \in Q} |\hat{f}(q) - f(q)| \quad (23)$$

⁴https://networks.skewed.de/net/wiki_talk

⁵<https://snap.stanford.edu/data/sx-stackoverflow.html>

⁶<https://snap.stanford.edu/data/web-NotreDame.html>

$$ARE = \frac{1}{|Q|} \sum_{q \in Q} \frac{|\hat{f}(q) - f(q)|}{f(q)} \quad (24)$$

where Q denotes the query set, and $f(q)$ and $\hat{f}(q)$ represent the ground truth and the estimated value returned by the sketch, respectively.

Parameters. We follow the same pre-training protocol as the Larval Phase of *Mayfly* [25], with specific adaptations to the training stream length to match the scale of our evaluation. For the main comparative experiments (§5.1) and robustness analysis (§5.2), we extend the synthetic stream length γ up to 600,000. This ensures the model is exposed to sufficient accumulated collisions and long-term dependencies, mimicking the conditions of large-scale real-world benchmarks. For ablation studies and parameter sensitivity (§5.3), we set γ to 60,000 to facilitate efficient exploration of the hyperparameter space. We build the distribution pool \mathcal{P} using Zipf distributions where the skewness parameter α ranges from 0.3 to 0.8. The total weight sum for tasks is set to range from 5 to 50 times the number of edges in the graph. We utilize 50 training steps per task and a learning rate of 5×10^{-4} . Regarding the model architecture, the representation network f_n in *Crane* is implemented as a Multi-Layer Perceptron (MLP) that maps the 32-dimensional binary representation space into a 64-dimensional embedding space: (1) a linear layer ($32 \rightarrow 16$) followed by Batch Normalization (BN) and ReLU activation; (2) an intermediate linear layer expanding the dimension ($16 \rightarrow 36$) followed by BN and ReLU; and (3) a final linear projection ($36 \rightarrow 64$) activated by ReLU.

5.1 Accuracy

We evaluate the accuracy of *Crane* on the fundamental task of **edge frequency estimation** against four baselines on real-world datasets, covering distinct traffic patterns ranging from heavy-tailed network flows to uniform web graphs. Table 1 reports the Average Relative Error (ARE) across varying stream lengths under a fixed 64KB memory budget.

Heavy-Tailed Traffic. The most significant challenges in our evaluation are posed by *CAIDA*, *WiKiTalk*, and *StackOverflow*, which exhibit highly skewed distributions and bursty interaction patterns. On *CAIDA*, flat sketches (TCM, GSS, Auxo) rapidly saturate, with errors exploding by orders of magnitude as the stream length grows from 2M to 27.1M. This collapse confirms the infrequent flow interference problem: when heavy hitters share the same counters as rare items, the resulting noise is catastrophic. While *Mayfly* mitigates this partially, it still yields high variance (ARE > 30). In stark contrast, *Crane* maintains a tightly bounded ARE (1.90 – 4.27) even as the stream volume increases by over 13×. Similarly, on the social interaction graphs *WiKiTalk* and *StackOverflow*, *Crane* outperforms the strongest baseline by a factor of roughly 9× to 60×. This robustness validates our core hypothesis: the hierarchical carry mechanism successfully isolates frequent flows in upper layers, preventing them from cannibalizing the capacity required for the “long tail” in lower layers.

Distinct Edge Stress Test. The *NotreDame* dataset represents a fundamentally different regime: it consists entirely of distinct edges with unit weights, eliminating heavy hitters and isolating the sketch’s ability to handle pure hash collisions. In this setting, every collision contributes directly to estimation error. Baselines

struggle significantly here; notably, hash-based methods like TCM and Auxo suffer from severe saturation. However, *Crane* achieves an ARE below 2.5 even at 1.5M distinct edges—an improvement of over 10× compared to *Mayfly*. This indicates that the hierarchical architecture is not solely dependent on skewness for its advantage. By distributing the load across multiple layers via learnable encoders, *Crane* effectively reduces the collision probability for any given edge, even in the absence of frequency disparity.

Moderate Scale. On the *Lkml* email corpus, which represents a more moderate scale and skewness, all methods perform relatively better than on the heavy-tailed datasets. Nevertheless, *Crane* continues to dominate, suppressing error rates to sub-unit levels (ARE < 1.0) for most stream lengths. The fact that *Crane* maintains a clear margin (improving by 4× to 55×) even on this “easier” workload suggests that its modeling capacity does not overfit to extreme conditions. Instead, it yields genuine gains in collision resolution and calibration that persist across varying scales.

Summary. Overall, the results in Table 1 demonstrate three consistent trends. First, *Crane* delivers uniformly lower error across all datasets, reducing ARE by approximately one order of magnitude compared to state-of-the-art neural methods. Second, the error growth with respect to stream length is significantly slower for *Crane*. This aligns with our automatic expansion strategy, which ensures that memory layers remain in a well-utilized but unsaturated regime. Finally, the performance benefits are consistent across diverse characteristics—from heavy-tailed IP traces to uniform web graphs—confirming that *Crane* learns a robust, dataset-agnostic summarization logic rather than memorizing specific workload patterns.

5.2 Robustness

To assess whether *Crane* learns a generalized summarization logic or simply overfits to the training distribution, we conduct a cross-distribution evaluation. We compare models pre-trained on **Uniform** weight distributions against our default models trained on **Zipfian** distributions, evaluating them on the five real-world datasets. Figure 5 illustrates the Average Absolute Error (AAE) across varying stream sizes.

Resilience to Distribution Mismatch. As evidenced by the comparison between light and dark bars in Figure 5, *Mayfly* exhibits extreme sensitivity to the training prior. When trained on Uniform distributions (dark blue) and applied to heavy-tailed real-world streams like *CAIDA* or *WiKiTalk*, *Mayfly*’s error typically explodes by two to three orders of magnitude. This confirms that flat neural sketches tend to memorize the statistical “shape” of the training data rather than learning an adaptive counting algorithm.

In contrast, *Crane* demonstrates significant robustness. While training on Uniform data naturally yields higher errors than the matched Zipfian training, the degradation is strictly bounded. Notably, on highly skewed datasets like *CAIDA* and *StackOverflow*, *Crane* trained on the “wrong” distribution (Uniform) still achieves AAE comparable to or better than *Mayfly* trained on the “correct” distribution (Zipf). This suggests that *Crane*’s performance is driven primarily by its hierarchical architecture and carry mechanism, which function effectively even when the learnable encoders are not perfectly tuned to the target skewness.

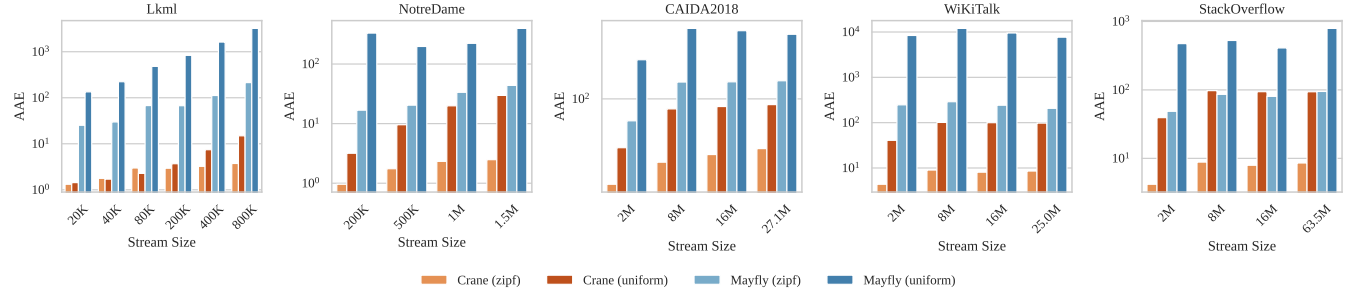


Figure 5: Robustness comparison.

Table 2: Ablation Studies on Memory Layer and Mini Batch Size (ARE)

Dataset	Memory Layer			Mini Batch Size		
	1	4	Δ	1	4	Δ
Lkml	5.91	5.74	+0.17	5.54	5.74	-0.20
NotreDame	15.62	15.07	+0.56	14.88	15.07	-0.18
CAIDA2018	93.14	77.48	+15.67	182.54	77.48	+105.06
WiKiTalk	89.51	76.81	+12.70	118.89	76.81	+42.09
StackOverflow	78.51	75.13	+3.38	181.47	75.13	+106.34
Average	56.54	50.04	+6.50	100.66	50.04	+50.62

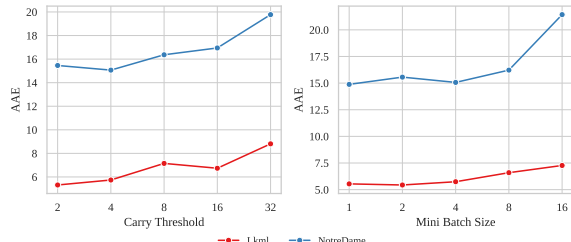


Figure 6: Accuracy of Crane under different hyperparameter settings on Lkml and NotreDame.

Generalization on Distinct Edges. The *NotreDame* dataset, which consists of distinct edges with unit weights, presents a unique case that structurally resembles a Uniform distribution. Intuitively, one might expect the Uniform-trained model to outperform the Zipf-trained one in this regime. However, Figure 5 reveals the opposite: *Crane* (Zipf) consistently achieves lower AAE than *Crane* (Uniform). We attribute this to the optimization dynamics: the Zipfian training tasks, with their high dynamic range frequencies, impose a stricter requirement on collision resolution. This forces the decoder to learn a sharper, more discriminative logic (approximating a precise \min operator) to isolate heavy hitters. This “sharpened” decoding capability generalizes better to rejecting background collision noise, even in distinct-edge streams, whereas Uniform training leads to smoother, less discriminative estimates that are more susceptible to hash collisions.

5.3 Ablation and Parameter Sensitivity

To rigorously quantify the contribution of each design component, we conduct ablation studies focusing on the depth of the hierarchical memory and the dynamics of the carry mechanism. Table 2

summarizes the Average Absolute Error (AAE) across datasets, while Figure 6 details the sensitivity to the carry threshold and mini-batch size.

Effectiveness of Hierarchical Memory. The core premise of Crane is that separating items vertically across layers reduces interference between heavy hitters and the long tail. To validate this, we compare the standard Crane configuration ($N = 4$ layers) against a collapsed “flat” variant ($N = 1$), where all capacity is forced into a single layer with equivalent total parameters.

As shown in the “Memory Layer” columns of Table 2, the hierarchical structure provides decisive benefits. On highly skewed datasets such as *CAIDA2018* and *WiKiTalk*, collapsing the hierarchy causes the AAE to degrade by 15.67 and 12.70 points, respectively. This sharp deterioration confirms the limitations of flat neural sketches discussed in §1: without vertical separation, the learnable encoders cannot sufficiently disentangle the overwhelming gradients of frequent items from the subtle signals of rare ones. By employing $N = 4$ layers, Crane effectively isolates these conflicting populations, reducing the average error by approximately 13% on average compared to the single-layer baseline.

Impact of Mini-Batch Strategy. Contrary to the intuition that strictly sequential processing ($b = 1$) yields the highest fidelity, Table 2 reveals that mini-batching ($b = 4$) reduces error on heavy-tailed datasets. We attribute this to the *noise-smoothing effect* of aggregation: summing basis matrices over a batch filters out transient collision noise, preventing premature promotions driven by instantaneous outliers. Given that the accuracy penalty on lighter datasets is negligible ($\Delta < 0.2$) while throughput improves drastically, we identify $b = 4$ as the optimal sweet spot for robustness and efficiency.

Sensitivity to Carry Threshold. The carry threshold θ governs the “viscosity” of the vertical flow; it determines how aggressive the model is in promoting items to higher layers. Figure 6 (Left) plots the AAE as θ varies from 2 to 32.

We observe a clear monotonic trend: lower thresholds consistently yield better accuracy. For instance, on *Lkml*, increasing θ from 2 to 32 nearly doubles the error (from ~ 5.3 to ~ 8.8). This validates the design motivation of the *Hierarchical Carry Mechanism* (§3.3). A lower θ facilitates the rapid “evacuation” of heavy hitters from the bottom layer. By aggressively promoting these items, Crane ensures that the bottom layer—which handles the vast majority of unique, low-frequency items—remains sparse and collision-free. Delaying promotion (high θ) forces large items to

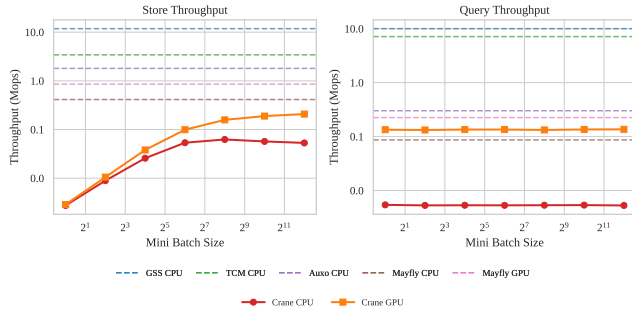


Figure 7: Throughput comparison.

linger in lower layers, where they unnecessarily consume capacity and collide with the tail. Consequently, we select a small constant (e.g., $\theta = 4$) to maximize separation efficiency.

5.4 Throughput

We evaluate the store and query throughput of Crane and compare it against the baseline methods. All throughput experiments are conducted on the *Lkml* dataset. Figure 7 reports the results on both CPU and GPU platforms.

Impact of Mini-Batch Size. Figure 7 (left) illustrates the storage throughput as a function of the mini-batch size b . Crane effectively leverages batch processing to amortize the overhead of neural encoding and memory updates. As b increases from 2^0 to 2^{12} , the throughput on CUDA improves by nearly two orders of magnitude, eventually saturating at approximately 0.2 Mops. This trend confirms that processing edges in mini-batches is essential for masking the latency of GPU kernel launches and maximizing the utilization of the neural encoders.

Throughput-Accuracy Trade-off. As observed in Figure 7, Crane exhibits lower throughput compared to traditional hash-based sketches and is slightly slower than the static neural baseline (Mayfly). This performance gap is expected and stems from two main factors: (1) the computational cost of the learnable encoders, which is inherently higher than simple hash functions; and (2) the limited parallelism imposed by our *carry-like promotion mechanism*. Unlike TCM, which allows fully parallel updates, Crane must enforce conservative consistency checks (as detailed in Algorithm 2) to correctly propagate heavy items through the hierarchy. However, this represents a deliberate strategic trade-off: we exchange raw processing speed for significantly higher estimation quality. While TCM achieves high speeds, it suffers from excessive collisions and poor accuracy on skewed streams. Crane, conversely, achieves orders-of-magnitude reductions in ARE and AAE (as shown in Table 1) by investing computational resources into a smarter hierarchical representation. Furthermore, a sustained throughput of ≈ 0.2 Mops is sufficient for a wide range of practical applications, including software-defined network monitoring, offline traffic analysis, and log summarization, where accuracy is often the primary bottleneck.

Query Performance. Figure 7(right) shows that the query throughput of Crane remains stable regardless of the memory configuration, maintaining a rate of approximately 0.15 Mops on GPU. This stability ensures predictable latency for retrieval operations, making

Table 3: Comparison of ARE for Node Flux Estimation between TCM and Crane

Dataset	Size	TCM	Crane	Impr.
Lkml	20k	77.70	0.86	90.3 \times
	40k	168.97	0.97	174.9 \times
	80k	297.92	1.22	245.0 \times
	200k	964.22	2.29	420.4 \times
	400k	1915.64	3.09	619.7 \times
	800k	3998.88	5.27	758.9 \times
NotreDame	200k	3669.35	3.01	1219.8 \times
	500k	8877.09	2.81	3162.1 \times
	1M	16664.30	14.98	1112.5 \times
	1.5M	24408.70	10.20	2393.5 \times

Crane a reliable choice for interactive analysis dashboards even as the underlying data volume grows.

5.5 Cases Studies

To demonstrate Crane’s capability beyond simple edge counting, we conduct a case study on **Node Flux Estimation**. Node flux (or weighted degree) measures the total incoming or outgoing weight of a specific node by aggregating the frequencies of all its incident edges. This metric is a fundamental primitive for downstream tasks, such as identifying “super-spreaders” in social networks or victim IPs in DDoS attacks. The objective of this experiment is to evaluate whether Crane can preserve such node-level structural properties under extreme memory compression, where traditional sketches often fail due to error accumulation.

Setup. We evaluate the Average Relative Error (ARE) of node flux estimates on two representative datasets: *Lkml* (interaction network) and *NotreDame* (web graph). We compare Crane against TCM, the most representative hash-based baseline. We omit other datasets from this table as baseline errors diverged to meaningless magnitudes ($> 10^4$).

Analysis. As shown in Table 3, Crane exhibits superior structural robustness. Traditional methods like TCM suffer from catastrophic hash collisions: a few high-degree nodes pollute the counters shared with varying low-degree nodes, driving the ARE up to 24,408 on *NotreDame*. In contrast, Crane leverages its hierarchical architecture to physically isolate heavy traffic in upper layers, preventing it from corrupting the estimates of tail nodes in lower layers. With an improvement ratio of up to 3,162 \times , Crane proves it can serve as a reliable substrate for complex graph analytics where structural fidelity is paramount.

6 CONCLUSION

In this paper, we propose Crane, a hierarchical neural sketch for graph stream summarization. Unlike existing methods, Crane utilizes a carry-like promotion mechanism to effectively separate frequent and infrequent items across layers, solving the issue of interference in limited memory environments. Further, Crane supports smooth automatic expansion, allowing it to handle streams of unknown or infinite length efficiently. Theoretical proofs confirm the space efficiency and error bounds of our design. Extensive evaluations show that Crane consistently outperforms SOTA methods, reducing estimation errors by over an order of magnitude.

REFERENCES

[1] Zhewei Wei, Xiaodong He, Xiaokui Xiao, Sibo Wang, Shuo Shang, and Ji-Rong Wen. Topppr: top-k personalized pagerank queries with precision guarantees on large graphs. In *Proceedings of the 2018 International Conference on Management of Data (SIGMOD)*, pages 441–456, 2018.

[2] Mengxi Ding and Shimin Chen. Efficient partitioning and query processing of spatio-temporal graphs with trillion edges. In *2019 IEEE 35th International Conference on Data Engineering (ICDE)*, pages 1714–1717, 2019.

[3] Qing Liu, Minjun Zhao, Xin Huang, Jianliang Xu, and Yunjun Gao. Truss-based community search over large directed graphs. In *Proceedings of the 2020 ACM SIGMOD International Conference on Management of Data*, pages 2183–2197, 2020.

[4] Anil Pacaci, Angela Bonifati, and M Tamer Özsu. Regular path query evaluation on streaming graphs. In *Proceedings of the 2020 ACM SIGMOD International Conference on Management of Data*, pages 1415–1430, 2020.

[5] Dhivya Eswaran, Christos Faloutsos, Sudipto Guha, and Nina Mishra. Spotlight: Detecting anomalies in streaming graphs. In *Proceedings of the 24th ACM SIGKDD International Conference on Knowledge Discovery & Data Mining*, pages 1378–1386, 2018.

[6] Yuncheng Wu, Ke Wang, Ruoyang Guo, Zhilin Zhang, Dan Zhao, Hong Chen, and Cuiping Li. Enhanced privacy preserving group nearest neighbor search. *IEEE Transactions on Knowledge and Data Engineering*, 33(2):459–473, 2019.

[7] Siddharth Bhatia, Arjit Jain, Pan Li, Ritesh Kumar, and Bryan Hooi. Mstream: Fast anomaly detection in multi-aspect streams. In *Proceedings of the Web Conference 2021*, pages 3371–3382, 2021.

[8] Siddharth Bhatia, Mohit Wadhwa, Kenji Kawaguchi, Neil Shah, Philip S Yu, and Bryan Hooi. Sketch-based anomaly detection in streaming graphs. In *Proceedings of the 29th ACM SIGKDD Conference on Knowledge Discovery and Data Mining*, pages 93–104, 2023.

[9] Samira Khodabandehlou and Alireza Hashemi Golpayegani. Fifraud: unsupervised financial fraud detection in dynamic graph streams. *ACM Transactions on Knowledge Discovery from Data*, 18(5):1–29, 2024.

[10] Shuhao Zhang, Juan Soto, and Volker Markl. A survey on transactional stream processing. *The VLDB Journal*, 33(2):451–479, 2024.

[11] Shipeng Qi, Bing Tong, Jiatao Hu, Heng Lin, Yue Pang, Wei Yuan, Songlin Lyu, Zhihui Guo, Ke Huang, Xujin Ba, et al. The ldbc financial benchmark: Transaction workload. *Proc. VLDB Endow.*, 18(9):3007–3020, 2025.

[12] Xiaolin Han, Yikun Zhang, Chenhao Ma, Lingyun Song, Reynold Cheng, and Xuequn Shang. Tempasd: Temporal anomalous subgraph discovery in large-scale dynamic financial networks. In *Proceedings of the 31st ACM SIGKDD Conference on Knowledge Discovery and Data Mining V*, 2, pages 826–837, 2025.

[13] Feng Zhao and Anthony KH Tung. Large scale cohesive subgraphs discovery for social network visual analysis. *Proc. VLDB Endow.*, 6(2):85–96, 2012.

[14] Yuchen Li, Zhipeng Bao, Guoliang Li, and Kian-Lee Tan. Real time personalized search on social networks. In *2015 IEEE 31st International Conference on Data Engineering (ICDE)*, pages 639–650, 2015.

[15] Xiangmin Zhou and Lei Chen. Event detection over twitter social media streams. *The VLDB journal*, 23(3):381–400, 2014.

[16] Kaiyu Chen, Dong Wen, Wenjie Zhang, Ying Zhang, Xiaoyang Wang, and Xuemin Lin. Querying structural diversity in streaming graphs. *Proc. VLDB Endow.*, 17(5):1034–1046, 2024.

[17] Peixiang Zhao, Charu C Aggarwal, and Min Wang. gsketch: On query estimation in graph streams. *Proc. VLDB Endow.*, 5(3), 2011.

[18] Nan Tang, Qing Chen, and Prasenjit Mitra. Graph stream summarization: From big bang to big crunch. In *Proceedings of the 2016 International Conference on Management of Data*, pages 1481–1496, 2016.

[19] Xiangyang Gou, Lei Zou, Chenxingyu Zhao, and Tong Yang. Fast and accurate graph stream summarization. In *2019 IEEE 35th International Conference on Data Engineering (ICDE)*, pages 1118–1129, 2019.

[20] Jihoon Ko, Yunbum Kook, and Kijung Shin. Incremental lossless graph summarization. In *Proceedings of the 26th ACM SIGKDD International Conference on Knowledge Discovery & Data Mining*, pages 317–327, 2020.

[21] Xiangyang Gou, Lei Zou, Chenxingyu Zhao, and Tong Yang. Graph stream sketch: Summarizing graph streams with high speed and accuracy. *IEEE Transactions on Knowledge and Data Engineering*, 35(6):5901–5914, 2022.

[22] Ming Chen, Renxiang Zhou, Hanhua Chen, Jiang Xiao, Hai Jin, and Bo Li. Horae: A graph stream summarization structure for efficient temporal range query. In *2022 IEEE 38th International Conference on Data Engineering (ICDE)*, pages 2792–2804, IEEE, 2022.

[23] Ming Chen, Renxiang Zhou, Hanhua Chen, and Hai Jin. Scube: Efficient summarization for skewed graph streams. In *2022 IEEE 42nd International Conference on Distributed Computing Systems (ICDCS)*, pages 100–110, 2022.

[24] Zhiqiu Jiang, Hanhua Chen, and Hai Jin. Auxo: A scalable and efficient graph stream summarization structure. *Proc. VLDB Endow.*, 16(6):1386–1398, 2023.

[25] Yuan Feng, Yukun Cao, Wang Hairu, Xike Xie, and S Kevin Zhou. Mayfly: a neural data structure for graph stream summarization. In *The twelfth International Conference on Learning Representations*, 2024.

[26] Yukun Cao, Yuan Feng, and Xike Xie. Meta-sketch: A neural data structure for estimating item frequencies of data streams. In *Proceedings of the AAAI Conference on Artificial Intelligence*, volume 37, pages 6916–6924, 2023.

[27] Yuan Feng, Yukun Cao, Hairu Wang, Xike Xie, and S Kevin Zhou. Lego sketch: A scalable memory-augmented neural network for sketching data streams. *arXiv preprint arXiv:2505.19561*, 2025.

[28] Tong Yang, Jie Jiang, Peng Liu, Qun Huang, Junzhi Gong, Yang Zhou, Rui Miao, Xiaoming Li, and Steve Uhlig. Elastic sketch: Adaptive and fast network-wide measurements. In *Proceedings of the 2018 Conference of the ACM Special Interest Group on Data Communication*, pages 561–575, 2018.

[29] Yang Zhou, Tong Yang, Jie Jiang, Bin Cui, Minlai Yu, Xiaoming Li, and Steve Uhlig. Cold filter: A meta-framework for faster and more accurate stream processing. In *Proceedings of the 2018 International Conference on Management of Data*, pages 741–756, 2018.

[30] Graham Cormode and Shan Muthukrishnan. An improved data stream summary: the count-min sketch and its applications. *Journal of Algorithms*, 55(1):58–75, 2005.

[31] Moses Charikar, Kevin Chen, and Martin Farach-Colton. Finding frequent items in data streams. *Theoretical Computer Science*, 312(1):3–15, 2004.

[32] Cristian Estan and George Varghese. New directions in traffic measurement and accounting: Focusing on the elephants, ignoring the mice. *ACM Transactions on Computer Systems*, 21(3):270–313, 2003.

[33] Jason Weston, Sumit Chopra, and Antoine Bordes. Memory networks. *arXiv preprint arXiv:1410.3916*, 2014.

[34] Alex Graves, Greg Wayne, Malcolm Reynolds, Tim Harley, Ivo Danihelka, Agnieszka Grabska-Barwińska, Sergio Gómez Colmenarejo, Edward Grefenstette, Tiago Ramalho, John Agapiou, et al. Hybrid computing using a neural network with dynamic external memory. *Nature*, 538(7626):471–476, 2016.

[35] Ilya Loshchilov and Frank Hutter. Decoupled weight decay regularization. *arXiv preprint arXiv:1711.05101*, 2017.

[36] Yulin Xu and Minghui Zhou. A multi-level dataset of linux kernel patchwork. In *Proceedings of the 15th international conference on mining software repositories*, pages 54–57, 2018.

[37] Ashwin Paranjape, Austin R Benson, and Jure Leskovec. Motifs in temporal networks. In *Proceedings of the tenth ACM international conference on web search and data mining*, pages 601–610, 2017.

[38] AH Jeong. Diameter of the world-wide web. *Nature*, 401:130–131, 1999.

APPENDIX

A MATHEMATICAL ANALYSIS

A.1 Proof of Logarithmic Space Efficiency (Lemma 1)

In Crane’s hierarchical mechanism, the frequency stored at layer l , denoted as v_l , conceptually represents the magnitude of the digit in a base- θ system. The total estimated frequency is approximately $\sum_{l=1}^L v_l \cdot \theta^{l-1}$. Considering the worst-case scenario where each layer is filled to its capacity (just below the threshold θ) before a carry occurs, the maximum capacity $C(L)$ of a Crane sketch with L layers is given by the geometric series:

$$C(L) \approx \sum_{l=1}^L (\theta - 1) \cdot \theta^{l-1} = (\theta - 1) \frac{\theta^L - 1}{\theta - 1} = \theta^L - 1 \quad (25)$$

To accommodate a stream where the maximum edge frequency is F_{max} , we require $C(L) \geq F_{max}$. Solving for L :

$$\theta^L \geq F_{max} + 1 \implies L \geq \log_\theta(F_{max} + 1) \quad (26)$$

Thus, the depth of the hierarchy L scales as $O(\log_\theta F_{max})$. Since the memory cost is linear with respect to L (i.e., $L \times |M|$), the total space complexity relative to the stream volume is logarithmic.

A.2 Proof of Logarithmic Amortized Complexity (Theorem 2)

Let L_t denote the number of active memory layers when the t -th edge e_t is inserted. According to the STORE operation, the encoder and memory update are performed for all L_t active layers. Thus, the insertion cost $T(e_t)$ is bounded by:

$$T(e_t) = O(L_t) + T_{carry}, \quad (27)$$

where T_{carry} is the cost of carry propagation. The carry propagation forms a convergent geometric series with an expected cost of $O(1)$. Therefore, the dominant term is $O(L_t)$. Due to the carry-like promotion with threshold θ , to accommodate a total weight W_t , the required depth is logarithmic: $L_t \approx O(\log_\theta W_t)$. Since $W_t \leq W_{total}$ for all t , the per-insertion cost is upper-bounded by $O(\log_\theta W_{total})$. Summing over the entire stream of N edges:

$$T_{total} = \sum_{t=1}^N T(e_t) \leq \sum_{t=1}^N C \cdot \log_\theta W_{total} = O(N \log_\theta W_{total}). \quad (28)$$

Dividing by N , the amortized complexity is $O(\log_\theta W_{total})$. Given $\theta \gg 2$, this remains a small constant.

A.3 Proof of Collision Probability Decay (Theorem 3)

Let e be a frequent item promoted up to layer k . The estimation accuracy depends on recovering its carried values. Let C_l be the event that edge e collides with another heavy item in layer l . Under Assumption 1, $P(C_l) \leq p$. For an error to persist up to layer k , collisions must occur simultaneously at every step of the promotion path. The joint probability is:

$$P(\text{Collision across } k \text{ layers}) = P\left(\bigcap_{l=1}^k C_l\right) = \prod_{l=1}^k P(C_l) \leq p^k \quad (29)$$

Since $p < 1$, the probability p^k decays exponentially as k increases. This implies that the significant “quotients” stored in higher layers are protected by an effective collision rate of p^k .

A.4 Proof of Residual Error Bound (Theorem 4)

The total error is decomposed into noise from the bottom layer and promoted layers.

- **Bottom Layer Error (Layer 1):** Stores only residual weights. The expected noise follows standard Count-Min logic:

$$\begin{aligned} E[\text{Noise}^{(1)}] &= \sum_{e' \neq e} P(\text{Collision}^{(1)}) \cdot (f(e') \pmod \theta) \\ &= \frac{1}{w} (W_{res} - f(e)^{(1)}) \approx \frac{W_{res}}{w} \end{aligned} \quad (30)$$

- **Higher Layers Error (Layer $l > 1$):** Based on Theorem 3, the collision probability is p^l . The expected noise is bounded by:

$$E[\text{Noise}^{(>1)}] \propto \sum_{l=2}^L p^l \cdot \theta^{l-1} \cdot W_{heavy} = p \cdot W_{heavy} \sum_{l=2}^L (p\theta)^{l-1} \quad (31)$$

Given the convergence condition $p \cdot \theta < 1$, the geometric series converges rapidly, suppressing error from heavy hitters.

Thus, $E[\text{Error}_{\text{Crane}}] \approx \frac{W_{res}}{w} + \epsilon_{high_layers}$, where the error is dominated by the small residual mass W_{res} .

A.5 Derivation of Learnable Encoder Orthogonality

Let A_u, A_v be basis matrices for edges u, v . Collision interference is proportional to $\langle A_u, A_v \rangle$. The training objective includes reconstruction loss \mathcal{L} . The gradient update for encoder parameters ϕ is:

$$\phi \leftarrow \phi - \eta \frac{\partial \mathcal{L}}{\partial \langle A_u, A_v \rangle} \frac{\partial \langle A_u, A_v \rangle}{\partial \phi} \quad (32)$$

For frequent items contributing to the loss, this optimization pressure actively drives $\langle A_u, A_v \rangle \rightarrow 0$. Thus, the network learns to avoid collisions for dominant items.

A.6 Proof of Variance Minimization (Theorem 5)

Let the estimate from layer l be a random variable Q_l with variance σ_l^2 . Lower layers have high variance (high collision), while higher layers are cleaner. The linear decoder optimizes weights $w = \{w_1, \dots, w_N\}$ to minimize MSE:

$$\min_w E[(y - \sum w_l Q_l)^2] = \min_w (\text{Bias}^2 + \text{Variance}) \quad (33)$$

This is equivalent to Inverse-Variance Weighting ($w_l \propto 1/\sigma_l^2$). The learnable decoder automatically assigns lower weights to noisy lower layers, ensuring $\text{Var}(\hat{y}_{\text{Crane}}) \leq \text{Var}(\hat{y}_{\text{Fixed}})$.

A.7 Proof of Interference Isolation (Theorem 6)

Problem Setup. Consider a target edge e_{target} with low frequency (an infrequent item) stored in a sketch of width w . We compare the expected estimation error caused by hash collisions in two architectures:

- **Flat Structure (e.g., Mayfly):** Accumulates the full frequency $f(e')$ of interfering edges into the same memory space.

- **Hierarchical Structure (Crane):** Decomposes frequency into $f(e') = q_{e'} \cdot \theta + r_{e'}$, storing $r_{e'}$ in the bottom layer and carrying $q_{e'}$ to higher layers.

Noise in Flat Structure. For a standard Count-Min style accumulation (which Mayfly approximates via additive memory updates), the estimator for e_{target} is $\hat{f}(e_{target}) = f(e_{target}) + \text{Noise}$. The expected error is proportional to the sum of weights of all other edges colliding in the same bucket:

$$\mathbb{E}[\text{Error}_{\text{Flat}}] = \frac{1}{w} \sum_{e' \neq e_{target}} f(e') \approx \frac{W_{\text{total}}}{w} \quad (34)$$

where $W_{\text{total}} = \|\mathbf{f}\|_1$. In heavy-tailed graph streams, W_{total} is dominated by a few heavy hitters, causing significant interference variance for small items.

Noise in Crane. As established in Theorem 4, assuming the convergence condition holds, the error in Crane is dominated by the noise in the bottom layer $M^{(1)}$. Due to the Hierarchical Carry Mechanism, any edge e' with frequency $f(e') \geq \theta$ is decomposed.

The memory $M^{(1)}$ only stores the residual component $r_{e'} = f(e') \pmod{\theta}$, where $0 \leq r_{e'} < \theta$. The expected error in the bottom layer is bounded by the sum of these residuals:

$$\mathbb{E}[\text{Error}_{\text{Crane}}^{(1)}] = \frac{1}{w} \sum_{e' \neq e_{target}} (f(e') \pmod{\theta}) \approx \frac{W_{\text{res}}}{w} \quad (35)$$

Comparison. The ratio of the expected errors is:

$$\mathcal{R} = \frac{\mathbb{E}[\text{Error}_{\text{Crane}}]}{\mathbb{E}[\text{Error}_{\text{Flat}}]} \approx \frac{W_{\text{res}}}{W_{\text{total}}} \quad (36)$$

For any edge e' where $f(e') \geq \theta$, we have $f(e') \pmod{\theta} \ll f(e')$. Specifically, for heavy hitters where $f(e') \gg \theta$, the stored weight in the bottom layer is negligible compared to their true frequency. Since graph streams typically follow a Zipfian distribution where the majority of total weight W_{total} comes from heavy hitters, the residual sum W_{res} effectively strips away the “heavy” components. Thus, $W_{\text{res}} \ll W_{\text{total}}$, proving that Crane physically isolates small items from the overwhelming noise of heavy hitters, a guarantee that flat structures cannot provide regardless of their encoding method. \square